Available online at www.sciencedirect.com

ScienceDirect

Green Energy & Environment xxx (xxxx) xxx

www.keaipublishing.com/gee

Research paper

Are Ni/ and Ni_5Fe_1/biochar catalysts suitable for synthetic natural gas production? A comparison with γ-Al_2O_3 supported catalysts

M. González-Castaño [a,*], C. Morales [b], J.C. Navarro de Miguel [c], J.H. Boelte [d], O. Klepel [d], J.I. Flege [b], H. Arellano-García [a]

[a] Department of Process and Plant Technology, Brandenburg University of Technology (BTU) Cottbus-Senftenberg, Platz der Deutschen 1, Cottbus, 03046, Germany

[b] Applied Physics and Semiconductor Spectroscopy, Brandenburg University of Technology Cottbus-Senftenberg, Konrad-Zuse-Strasse 1, Cottbus, 03046, Germany

[c] Department of Inorganic Chemistry, Institute of Materials Science of Seville, Consejo Superior de Investigaciones Cientificas (CSIC), Universidad de Sevilla (US), Avenida Américo Vespucio 49, Seville, 41092, Spain

[d] Institute of Materials Chemistry, Brandenburg University of Technology Cottbus–Senftenberg, Universitätsplatz 1, Senftenberg, D-01968, Germany

Received 14 January 2021; revised 6 May 2021; accepted 14 May 2021
Available online ■ ■ ■

Abstract

Among challenges implicit in the transition to the post–fossil fuel energetic model, the finite amount of resources available for the technological implementation of CO_2 revalorizing processes arises as a central issue. The development of fully renewable catalytic systems with easier metal recovery strategies would promote the viability and sustainability of synthetic natural gas production circular routes. Taking Ni and NiFe catalysts supported over γ-Al_2O_3 oxide as reference materials, this work evaluates the potentiality of Ni and NiFe supported biochar catalysts for CO_2 methanation. The development of competitive biochar catalysts was found dependent on the creation of basic sites on the catalyst surface. Displaying lower Turn Over Frequencies than Ni/Al catalyst, the absence of basic sites achieved over Ni/C catalyst was related to the depleted catalyst performances. For NiFe catalysts, analogous Ni_5Fe_1 alloys were constituted over both alumina and biochar supports. The highest specific activity of the catalyst series, exhibited by the NiFe/C catalyst, was related to the development of surface basic sites along with weaker NiFe–C interactions, which resulted in increased Ni^0:NiO surface populations under reaction conditions. In summary, the present work establishes biochar supports as a competitive material to consider within the future low-carbon energetic panorama.

Keywords: Biochar catalysts; Carbon catalysts; Ni catalysts; NiFe alloy; Bimetallic catalysts; Synthetic natural gas; CO_2 methanation

1. Introduction

The environmental consequences triggered by the continuous greenhouse emissions (GHE) due to the current fossil fuel energetic model had already upraised serious international concerns, In this regard, within the frame of Horizon Europe (HE), European policymakers are increasingly legislating to become carbon neutral by 2050 and limit the temperature rise below 2 °C [1]. Similarly, other global regions follow alike trends. The achievement of such carbon neutrality implies switching towards a novel circular paradigm in which wastes become valuable raw materials. Being the largest emitted GHE gas (37 Gt in 2019 [2]), CO_2 arises as a chief shackle to consider within the waste revalorization perspective. An indispensable portfolio on the CO_2 emissions abatement is the CO_2 hydrogenation to CH_4 ($CO_2 + 4H_2 = CH_4 + 2H_2O$, $\Delta H_{298} = -165.0$ kJ/mol). The high readiness level of thermo-catalytic processes along with the already existing natural gas gridlines sets the CO_2

* Corresponding author.
E-mail address: gonzalez@b-tu.de (M. González-Castaño).

https://doi.org/10.1016/j.gee.2021.05.007

methanation as a forthright approach for producing Synthetic Natural Gas (SNG).

Successful industrial implementations of CO_2 methanation units involve, along with low-priced H_2 available from renewable sources, active and stable catalysts. Another main challenge implicit in the energetic model transformation relates to the finite amount of available resources. Thus, the utilization of highly abundant and renewable materials for the catalytic systems results highly convenient. Dispersing metal particles over high surface porous materials allows lower metal contents by increasing the effective exposed area of the active phase [3]. It is known that the support's nature determines the resulting metal dispersion, thereby affecting the redox properties and overall catalyst performance [4]. The support acid–base properties also play an essential role in terms of catalyst activity and selectivity [5]. Being applied in several industrial processes, γ-Al_2O_3 is recognized as an excellent dispersing matrix with high thermal stability and optimal textural properties [6]. With significantly higher surface areas, templated materials such as zeolites or carbon supports arise as engaging alternatives. Being comparatively less studied than zeolites for CO_2 reduction processes, biochar-supported catalysts are shown capable of confining metal particles within the porous channels inhibiting the metal sintering in an effective manner [7]. The potentiality for tailoring the carbon porous structure as well as the functionalization achieved by surface treatments or heteroatom introduction explains the wide application of porous carbon supports as catalysts [8] or adsorbents [9]. From a sustainable perspective, the facile metal recovery allowed by carbon supports via gasification processes also supposes an important benefit to consider. This would indeed result in a fully recyclable catalyst, as far as carbon supports are produced from renewable materials such as sucrose.

Concerning the metal active phase, Ni-based formulations display fair activity to cost ratios along with superior availabilities than noble metal catalysts. Indeed, Ni metal sites are known capable of performing both H_2 dissociation and CO_2 activation [10]. Still, the deactivation issues related to carbon deposits and Ni sintering frequently described for Ni metal catalysts results in compromised performance and durability. Recently, Wu et al. [11] described Ni encapsulated into graphene-like carbon supports as an active and stable catalyst due to the mitigation of Ni sintering allowed by physically confined Ni particles within the porous structure. On achieving enhanced systems, the addition of adequate amounts of a secondary metal has been proved an effective strategy. Over the Ni/Al_2O_3 commercial catalyst for CO_2 methanation, the incorporation of metal oxides like CeO_2 [12,13], MnO_2 [14] or Fe_2O_3 [15] results in enhanced activities. The improvement attained by bimetallic formulations are usually associated with improved CO_2 absorptions [16] and inhibited cooking phenomena [17]. For instance, Kim et al. [18] stated that NiFe alloys evolve to Ni-enriched NiFe alloys with surface FeO domains capable of removing carbon deposits via redox reactions. According to density function theory (DFT) investigations conducted over Ni–Cu, Ni–Fe and Ni–Co catalysts by Ray et al. [19], the superior CO_2 methanation rates exhibited by Ni–Fe systems were associated to the lower number of d-density of states (d-DOS) at the Fermi level. Indeed, the catalytic benefits provided by NiFe alloys for CO_2 methanation reaction has been described for several metal supported formulations [20]. For $Ni–Fe/Ce_xZr_{1-x}O_2$ multicomponent systems, the Fe addition resulted in improved performances within the lower temperature range [21]. Similar observations were made for $Ni–Fe/ZrO_2$ catalysts in [22] where the enhanced catalyst activity of Ni–Fe systems was ascribed to easier CO_2 and H_2 activation processes. Besides, the enhanced CO_2 conversion and selectivites towards CH_4 attained by Ni–Fe catalysts has been also related to optimal CO activation energies [23,24], moderate absorptions of formate intermediates [25] and hindered oxidations of Ni^0 active phases [26].

This work investigates the prospective of biochar-supported Ni catalysts for obtaining SNG via CO_2 methanation reaction. To establish a meaningful comparison, γ-Al_2O_3 based catalysts were used as reference systems. Although a direct parallelism is not an easy task due to the different supports' nature, this work avoids the uncertainties derived from the previously reported works where different synthesis methods, feedstock compositions and reaction conditions are employed. Thus, high surface biochar and γ-Al_2O_3 supports were compared over different Ni catalysts' formulations, namely: Ni and Ni–Fe, for CO_2 methanation reaction. The relative metal contents were carefully selected according to previously reported optimizations [27,28]. The metal contents intended for the catalysts series were 10% Ni and 10% Ni - 3% Fe. Given the attained outcomes, the present study shows that suitable catalyst formulations render Ni–Fe biochar-supported catalysts a competitive and sustainable system for CO_2 methanation.

2. Material and methods

2.1. Synthesis of materials

Silica gel (CWK Bad Köstritz GmbH) employed as a template was infiltrated with aqueous solutions of sucrose (65 wt.-%) as carbon precursors. The resulting template and precursor mixture was carbonized in an turbular quartz furnace under N_2 atmosphere at 600 °C. Up to three infiltration and carbonization cycles were performed in order to fill the remaining pore volume of the template with carbon. Subsequently, the obtained carbon/template-composites where heat-treated at 900 °C also in N_2 to remove unstable surface groups. Then, the template was dissolved with hydrofluoric acid (40%). Finally, the resulting biochar matrix was repeatedly washed in deionized water until neutrality and dried at 120 °C in air. Biochar materials are also referred as carbon materials.

For the prepared samples, the nominal metal contents intended were 10 wt.% Ni and 3 wt.% Fe. The metals were incorporated over γ-Al_2O_3 (Sasol) and carbon supports via wetness impregnation employing the following precursors' $Ni(NO_3)_2 \times 6H_2O$ (98%) and $Fe(NO_3)_3 \times 6H_2O$ (99%). Thus,

Please cite this article as: M. González-Castaño et al., Are Ni/ and Ni_5Fe_1/biochar catalysts suitable for synthetic natural gas production? A comparison with γ-Al_2O_3 supported catalysts, Green Energy & Environment, https://doi.org/10.1016/j.gee.2021.05.007

adequate amounts were dissolved in ethanol aqueous solutions and added over their corresponding supports. Afterward, the solvent was evaporated under reduced pressure at 70 °C. The resulting solids were dried overnight at 120 °C. Different annealing procedures were employed for carbon and Al_2O_3 supported catalysts. Al_2O_3 catalysts were calcined in air at 500 °C for 4 h employing 10 °C/min heating ramps. Carbons were annealed at 300 °C during 8 h under diluted H_2/N_2 atmospheres according to the optimization performed by Gandia et al. [29] for Ni catalysts supported over carbon supports. The prepared catalysts 10 wt.% Ni/γ-Al_2O_3, 10 wt.% Ni-3wt.% Fe/γ-Al_2O_3, 10 wt.% Ni/Biochar and 10 wt.% Ni-3wt.% Fe/Biochar were labeled Ni/Al, NiFe/Al, Ni/C, and NiFe/C, correspondingly.

2.2. Characterization techniques

The chemical composition of the samples was analyzed by Inductively Coupled Plasma Mass Spectrometer (ICP-MS) employing nitric acid for digesting the samples. The textural properties were evaluated over the samples previously degassed at 200 °C by N_2 physisorption measurements performed in ASAP 2020 Micromeritics devices. X-ray diffraction (XRD) measurements were carried out with a Bruker D2 Phaser instrument using the Cu K_α radiation (λ = 1.5418 Å) as a source. XRD measurements were taken in the 2θ range = 20−80° using a step size of 0.05° and step time of 1s. The lattice parameter was estimated employgin Braggs' law for fcc structures (Eq. (1)) where *h,k,l* are the miller indexs of the referred diffraction plane, λ accounts for the wavelength of Cu filament (1.5405 Å) and θ relates to the peak position.

$$a = \frac{\sqrt{(h^2 + k^2 + l^2)}\lambda}{2sin\theta} \quad (1)$$

Raman measurements were performed employing a Raman microscope (DXR Raman microscope, Thermo Fischer Scientific) with a high-resolution grating (1800 lines/mm). A green laser excitation (532 nm) was used to excite the sample through a 50 × - objective. Transmission electron microscopy (TEM) was performed in an FEI Talos electron microscope suited with a Field Emission filament. Micrographs were taken employing 200 kV acceleration voltage and a side-mounted Ceta 16 M camera. For establishing the particle size distribution, close to 200 particles from different micrographs were considered. According to the methodology proposed elsewhere [30], the metal dispersion (D) was estimated employing *equation* 2 where n_s and n_t account for the surface and total number of atoms, respectively. The number of atoms per unit area was calculated supposing equal proportions of (111) (100) and (110) planes.

$$D = \frac{n_s}{n_t} \quad (2)$$

X-Ray Photoelectron Spectroscopy (XPS) measurements were performed with an Omnicron EA 125 hemispherical electron analyzer using Mg Kα to avoid overlap of the main photoemission and Auger signals from Ni and Fe with the Ni 2p, Fe 2p and K 2p regions of interest. The pass energy was set to 20 eV, giving an overall resolution of about 1.1 eV. The charge effects were corrected by adjusting the mainline of the NiO spectra fitting at 854.5 eV [31]. The spectra have been fitted after Shirley's background removal and using the XPS Peak software, version 4.1. In the case of NiO, the separation between peaks (Metallic, Main, Surface, Nonlocal, and Satellite components), the relative intensity and FWHM (Main, Surface, and Nonlocal) have been fixed for all Ni $2p_{3/2}$ spectra and supports [31]. The Fe 2p spectra have been fitted following the model suggested in [32].

The H_2-Temperature Programmed Reductions (H_2-TPR) tests were performed in a Pulsar ChemBET (AntonPar) device equipped with a TCD detector. H_2-TPR was recorded up to 900 °C with 10 °C/min heating ramps using 5% H_2/N_2 gas mixtures. CO_2-Temperature Programmed Desorption (CO_2-TPD) measurements were also carried out Pulsar ChemBET (AntonPar) device. For CO_2-TPD tests, the samples were pre-reduced at 600 °C in H_2 presence and subsequently, cooled down in inert He atmospheres. CO_2 was absorbed until saturation and afterward, desorbed at room temperature under He gas flows. The completion of the CO_2 absorption and desorption at room temperature was followed by a mass spectrometer. CO_2-TPD experiments were recorded with the temperature increasing at 10 °C/min in He gas flow.

2.3. Catalytic activity measurements

Catalytic activity tests were performed in a Hastelloy tubular reactor (inner diameter = 0.9 mm). The composition of the inlet/outlet gas mixture was evaluated by an ABB gas analyzer suited with URAS 26 and CALDOS 25 units. The catalytic tests were performed at 60 L/gh employing 100 mg of catalyst (ϕ = 250–500) diluted with SiC up to bed volumes of 1 cm^3. The catalyst performance was analyzed using 100 mg of catalysts. Employing H_2:CO_2 = 4 ratios, the feed stream was composed of 12 vol.% CO_2 and 40 vol.% CO_2 balanced in N_2. The effect of the H_2:CO_2 ratio and space velocity was evaluated at 400 °C. Once steady-state conditions were achieved, CO_2 conversion and CH_4/CO selectivity's were calculated according to Eqs (2)–(4), respectively. In addition, Turn Over Frequencies (TOFs, s^{-1}) were estimated according to Eq. (6) where D accounts for the metal dispersion estimated from the TEM micrographs.

$$\%\ CO_2\ conversion = \frac{F_{CO2,\,in} - F_{CO2,\,out}}{F_{CO2,\,in}} \times 100 \quad (3)$$

$$\%\ Selectivity\ CH_4 = \frac{F_{CH4,\,out}}{F_{CH4,\,out} + F_{CO,\,out}} \times 100 \quad (4)$$

$$\%\ Selectivity\ CO = \frac{F_{CO,\,out}}{F_{CH4,\,out} + F_{CO,\,out}} \times 100 \quad (5)$$

Please cite this article as: M. González-Castaño et al., Are Ni/ and Ni_5Fe_1/biochar catalysts suitable for synthetic natural gas production? A comparison with γ-Al_2O_3 supported catalysts, Green Energy & Environment, https://doi.org/10.1016/j.gee.2021.05.007

$$TOFs = \frac{mol_{CO2,converted}}{s \cdot mol_{Ni} \cdot D} \quad (6)$$

3. Results

3.1. Chemical composition and textural properties

The N_2 adsorption–desorption isotherms exhibited by as-prepared samples are presented in Fig. 1. All samples exhibited the H1-type hysteresis characteristic of mesoporous carriers, in which the steep adsorption volume increase is related to pore condensation. The surface areas and pore structure (Fig. S1) displayed by all the samples were dominated by their corresponding supports. The BET surface area and pore volume values are listed in Table 1. Biochar based samples exhibit significantly higher surface areas than bare Al_2O_3. Compared to the supports, the addition of metals reduces the resulting surface areas, being this decrease more pronounced for the NiFe samples. Concerning the pore volumes, minor decrements were observed for the Al_2O_3 based catalysts. The metals impregnation on the biochar support, however, results in noticeable pore volume diminutions. Besides, the fraction of μ-pores initially exhibited by biochar support is markedly reduced. The surface area and pore volume decrements can be associated with metal particles partially blocking the pores of the support. The chemical composition of the samples obtained by ICP analysis is also shown in Table 1. Close to nominal metal contents were attained for all samples. Ni:Fe molar ratios of 3.9 and 3.6 were obtained for NiFe/Al and NiFe/C, respectively.

3.2. XPS analysis

Nature and surface exposure of the elements present in the as-prepared catalysts was evaluated by XPS. For Al_2O_3 and biochar based catalysts, Fig. 2 displays the Ni 2p (Fig. 2A and B) and Fe 2p (Fig. 2C and D) spectra. For NiO, Ni 2p core spectra were modeled in terms of Metallic, Main, Surface, Nonlocal, and Satellite components [31]. The Ni surface (I_S) to bulk (I_M) ratio observed for the prepared catalysts is also indicated in Fig. 2. For the as-prepared samples, mostly NiO species were found on the surface. The different support nature does not provide any difference in terms of Ni reduction extent for the as-synthesized samples. The major contribution of the surface component noted in the Ni 2p spectra underlines NiO oxide is nanostructured [33].

Table 1
Textural properties and chemical composition of the synthesized samples.

	BET (m^2/g)	V_{pore} (cm^3/g)	$V_{\mu\text{-pore}}$ (cm^3/g)	Ni wt.%	Fe wt.%
Al_2O_3	202	0.49	–	–	–
Ni/Al	168	0.41	–	9.79	–
NiFe/Al	163	0.41	–	9.69	2.35
C	895	1.89	0.33	–	–
Ni/C	745	1.58	0.21	9.77	–
NiFe/C	712	1.50	0.17	10.20	2.76

The presence of Fe increases I_m/I_s ratio suggesting increased NiO bulk contributions for the bimetallic systems. Employing *operando* XAS and XRD techniques, Serrer et al. [26] associated the benefits of NiFe alloy with a NiO superior resistance towards oxidation in presence of CO_2. For the as-prepared samples, such effect was particularly evidenced in the case of Al_2O_3 where the Fe presence hinders the Ni total oxidation. Concerning to Fe species, a Fe^{2+} and Fe^{3+} mixture was detected in all the solids. From the estimated Fe^{3+}/Fe^{2+} ratios, relative larger amounts of Fe^{3+} were exhibited by both NiFe/Al and NiFe/C catalysts.

3.3. XRD and TEM study

XRD diffractograms obtained for the prepared catalysts did not exhibit clear diffraction lines attributed to Ni nor Fe species indicating that, prior the reduction treatment, Ni and Fe metal oxides presented particle sizes below the 4 nm (Fig. S2), in line with XPS results. Besides, Raman spectra obtained biochar support and corresponding catalysts (Fig. S3) evidenced that the metal incorporation did not entail significant changes of the structural features exhibited by the biochar support. Fig. 3 presents the XRD data obtained for the reduced catalysts. Both Al_2O_3 and carbon supports are included for sake of clarity. After reducing in H_2 presence at 600 °C, the comparison with the bare alumina support advocated a certain contribution attributed to $NiAl_2O_4$ species for Ni/Al and NiFe/Al samples. Regarding the extent of $NiAl_2O_4$ formation, no significant differences were discerned between Ni/Al and

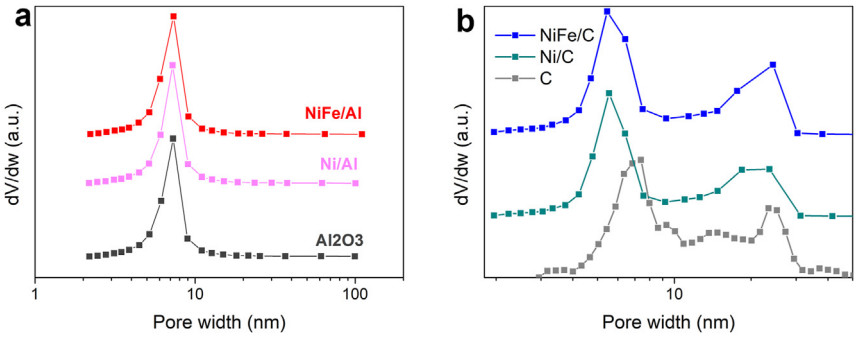

Fig. 1. Adsorption desorption isotherms of the as-prepared: a) Ni/Al and NiFe/Al and b) Ni/C and NiFe/C catalysts.

Please cite this article as: M. González-Castaño et al., Are Ni/ and Ni_5Fe_1/biochar catalysts suitable for synthetic natural gas production? A comparison with γ-Al_2O_3 supported catalysts, Green Energy & Environment, https://doi.org/10.1016/j.gee.2021.05.007

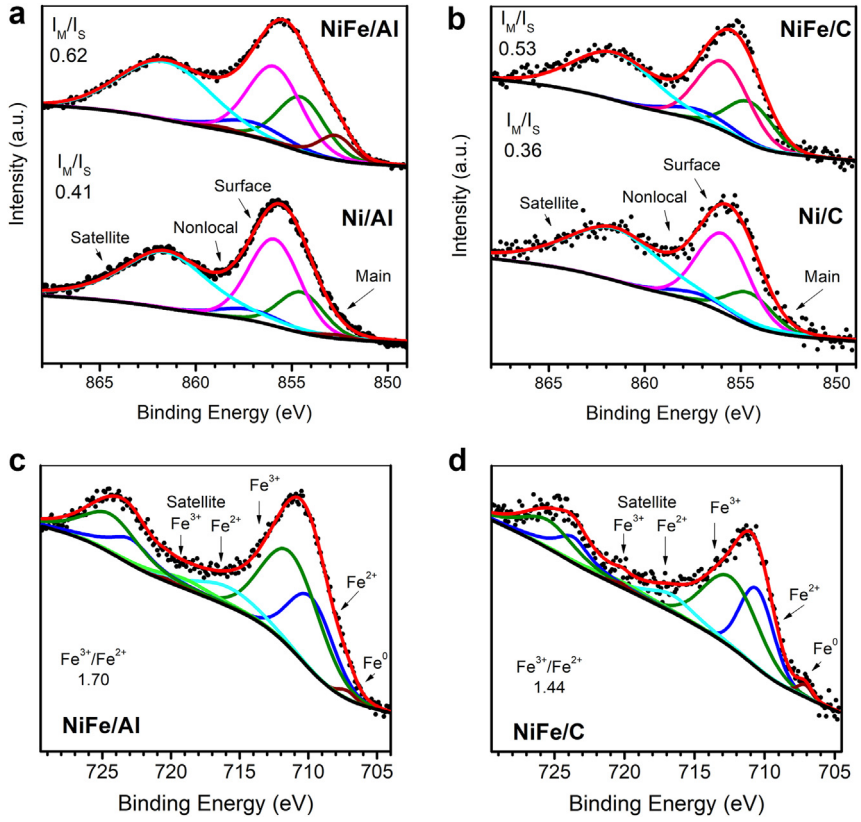

Fig. 2. XPS spectra obtained for as-prepared samples: a) Ni $2p_{3/2}$ for Ni/Al and NiFe/Al; b) Ni $2p_{3/2}$ for Ni/C and NiFe/C; c) Fe 2p for NiFe/Al; d) Fe 2p for NiFe/C catalysts.

NiFe/Al samples. Besides, the absence of peaks attributed to iron oxides suggests well-dispersed iron oxide phases for all catalysts. No clear signs attributed to NiO species were discerned for alumina catalysts. For carbon catalysts, diffraction lines at $2\theta = 37$ and 63° evidenced the presence of NiO species. On the other hand, sharp Ni^0 diffractions lines were discerned for all reduced samples. For NiFe-supported catalysts, shifts towards lower 2θ angles of Ni^0 diffraction peaks indicated lattice expansions suggesting the constitution of Ni–Fe alloys. Ni–Fe substitutional solid solution should indeed result in lattice parameter expansions due to the higher ionic radius of Fe (0.645 for Ni and 0.6690 Å for Fe). The lattice parameters were estimated from the (200) crystal plane placed around 51.8° (where no diffraction lines from γ-Al_2O_3 nor biochar supports are observed). Thus, Ni/C and Ni/Al respectively exhibited lattice parameters of 3.528 Å and 3.525 Å being those similar to the characteristic lattice parameter reported for pure fcc Ni (3.524 Å) [34]. Assuming cubic crystal structures, similar lattice expansions were exhibited by NiFe alloys for both NiFe/C and NiFe/Al bimetallic catalysts (3.546 and 3.545 Å). According to Vegard's law [35], Ni_5Fe_1 alloys were constituted for NiFe/C and NiFe/Al catalysts.

The average crystallite sizes estimated by Scherrer's equation for Ni^0 and NiFe alloys are presented in Table 2. Compared to Ni/Al sample which exhibited Ni^0 crystallite sizes around 9 nm, Ni/C catalysts exhibited significantly higher Ni^0 crystal sizes (22 nm). Considering the analogous synthesis method and the higher surface areas displayed by char support, weaker Ni–C support interactions might explain the higher extent of Ni^0 agglomeration during the reduction process. Furthermore, the lattice distortions provoked by the constitution of Ni–Fe solid solutions result in hindered crystal growth [36]. Hence, NiFe average crystal sizes of 10 and 5 nm were observed for NiFe/C and NiFe/Al catalysts respectively. Therefore, the nature of the support entails variations on the resulting crystal sizes with larger Ni, NiO, and NiFe crystallites developed over biochar support.

Fig. 4 shows the TEM micrographs obtained for the reduced catalysts along with their corresponding particle size distributions. Compared to biochar catalysts, alumina supported catalysts exhibited narrower particle distribution and lower particle sizes being the latter already intuited in XRD measurements. As established by Santos et al. [37,38], the nucleation and anchoring of metal particles over carbon surfaces mostly occurs through oxygenated groups. The larger particles sizes systematically found for biochar based systems could be indeed associated to the lower concentrations of oxygenated compounds attained during the reductive catalyst pre-treatment [39]. Table 3 shows the average particle size and metal dispersion obtained from TEM analysis. For both supports, the constitution of Ni–Fe bimetallic catalysts resulted on similar particle size

Please cite this article as: M. González-Castaño et al., Are Ni/ and Ni_5Fe_1/biochar catalysts suitable for synthetic natural gas production? A comparison with γ-Al_2O_3 supported catalysts, Green Energy & Environment, https://doi.org/10.1016/j.gee.2021.05.007

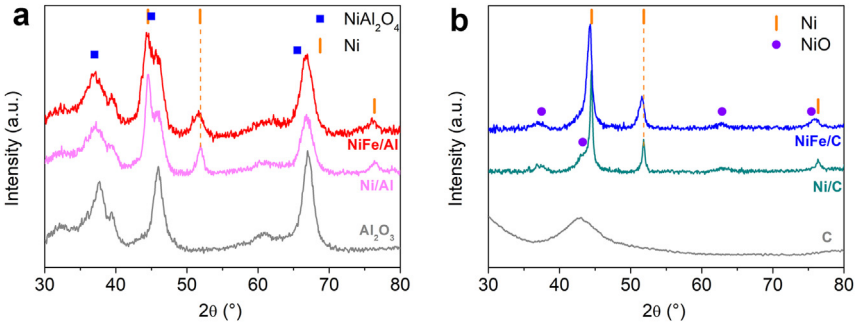

Fig. 3. XRD data of the reduced catalysts: a) Ni/Al and NiFe/Al and b) Ni/C and NiFe/C catalysts.

reductions compared to the monometallic samples. For Ni–Fe bimetallic catalysts, Fe might act as textural promoter that hinders Ni sintering processes and attains higher amounts of exposed Ni active sites [34].

3.4. H_2-TPR and CO_2-TPD analysis

The reducibility of the samples was analyzed by H_2-TPR. As shown in Fig. 5, the reduction profiles drawn by Ni supported catalysts depend on the strength of the metal-support interaction and metal particle size. Generally, larger NiO particles and weaker metal-support interactions result in lower reduction temperatures. Over the analyzed catalysts, higher reduction temperatures were systematically displayed by alumina supported catalysts, agreeing with the lower particle sizes observed in TEM analysis. The significantly stronger metal support interactions established between Ni metal and Al_2O_3 support should be related to the higher dispersions attained. Compared to biochar catalysts, significantly wider reduction profiles were also shown by Al_2O_3 supported catalysts. In this sense, Ni/Al exhibited a reduction profile composed of two reduction peaks underlining different Ni environments. NiO reduction peaks around 600 °C are associated with Ni^{2+} species strongly interacting with Al_2O_3. The higher temperature reduction peak observed around 800 °C can be attributed to nickel aluminate ($NiAl_2O_4$) species, also detected in XRD diffractograms [40]. On the other hand, biochar catalysts exhibited a single NiO reduction peak proposing a single redox behavior. The NiO reductions observed around 460 °C for biochar-supported catalysts are usually associated to free metal oxide particles poorly interacting with the support.

Table 2
For reduced samples, Ni crystallite sizes (Ni_{CS}) from XRD. Ni particle sizes (Ni_{PS}) and dispersion (Ni_D) from TEM.

	Ni_{CS} (nm)	Ni_{PS} (nm)	Ni_D (%)
Ni/Al	9	8	13
NiFe/Al	5	6	18
Ni/C	22	13	9
NiFe/C	10	11	10

For Al_2O_3 and C supported catalysts, the iron incorporation resulted in H_2-consumptions at temperatures around 400 °C. Iron oxide reductions take place in a stepwise manner according to the reaction scheme: $Fe_2O_3 \rightarrow Fe_3O_4 \rightarrow FeO \rightarrow Fe$ [41]. The reduction of $Fe_2O_3 \rightarrow Fe_3O_4$ accounts for the reduction peak observed at around 400 °C. Although not clearly observed, subsequent Fe reductions cannot be ruled out. Besides, Fe addition does not entail significant changes in the Ni reduction temperatures for none of the supports. In agreement with similar Ni–Fe systems [18], NiFe/Al sample exhibited consecutive Fe_2O_3, NiO, and $NiAl_2O_4$ reductions observed as the temperature increased. NiFe/C exhibited a narrower reduction peak compared to the bare Ni/C catalyst. Similar reduction profiles have been associated with the intimate contact between Ni and Fe species constituting NiFe alloys [42]. The H_2 quantification estimated assuming Ni^{2+} and Fe^{3+} total reductions is presented in Table 3. The Ni capability for performing H_2 spillover processes, from the metal to the support, explains the certain over-consumptions discerned for all the samples. The higher mol H_2/mol Ni ratios observed for the biochar-supported samples might be related to a higher number of reactive sites coordinately unsaturated originated from the decomposition of surface oxygen groups.

The surface basicity of the samples was analyzed by CO_2-TPD followed by a mass spectrometer (Fig. 6). Indeed, the surface basicity has been related with enhanced capacities for the adsorption and activation of CO_2 molecules [5]. Remarkable differences in terms of desorption profiles and species desorbed were observed as a function of the catalyst support. While all the samples desorbed CO_2 species, Ni/C and NiFe/C catalysts also exhibited important amounts of CO species. CO_2 desorption profiles ranging from ca. 120–400 °C were observed for alumina supported catalysts. Concerning the Ni/Al catalyst, NiFe/Al sample shown wider desorption profiles slightly shifted towards higher temperatures.

Biochar-supported catalysts exhibited the majority of the desorbed species above 400 °C with a small contribution around 150 °C, most likely associated with biochar support (Fig. S4). For biochar supports, CO/CO_2 desorption's are generally related with two types of surface oxygen groups with different acid-base character: i) acidic oxygen groups decompose into CO_2 molecules and might be associated

Please cite this article as: M. González-Castaño et al., Are Ni/ and Ni_5Fe_1/biochar catalysts suitable for synthetic natural gas production? A comparison with γ-Al_2O_3 supported catalysts, Green Energy & Environment, https://doi.org/10.1016/j.gee.2021.05.007

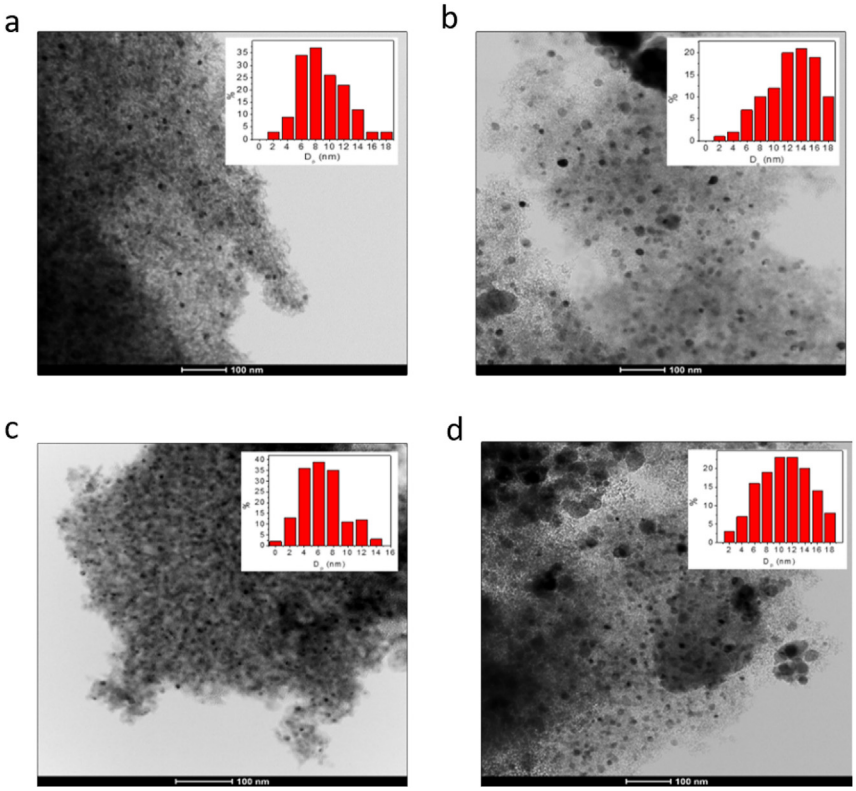

Fig. 4. TEM micrographs and particle size distribution obtained for reduced: a) Ni/Al; b) Ni/C; c) NiFe/Al and d) NiFe/C.

with carboxyl (below 623 °C) and carboxylic anhydrides and lactones (600–800 °C) species; ii) basic oxygen surface groups with associated phenols, quinones, and carbonyl groups decompose into CO species [43]. It should be noted that the decomposition of carboxylic anhydrides results in simultaneous CO and CO_2 evolutions. Fig. S3 shows the CO_2-TPD obtained for pre-reduced biochar support. Compared to Ni/C and NiFe/C catalysts, neglectable amounts of CO_2 and CO species were desorbed by the reduced biochar support. The superior amounts of CO/CO_2 species desorbed after the metals impregnation over the biochar supports evidenced enhanced concentration of basic and acid sites on the catalyst surface [44]. Thus, CO_2 peaks at ca. 150 and 450 °C must be related to acidic surface sites while CO species evolved at temperatures above 550 °C are associated with basic oxygen surface sites.

Table 3 shows the quantification of the CO_2-TPD experiments. For Al_2O_3 supported catalysts, the surface basicity was evaluated considering the amount of CO_2 species desorbed. For Ni/C and NiFe/C catalysts, the surface basicity was estimated uniquely from the CO species associated with basic surface sites. Under these assumptions, alumina catalysts evidenced higher surface basicity compared to their homologous biochar ones. The analogous amounts of CO and CO_2 desorbed by the Ni/C catalyst suggest acidic oxygen sites (with associated carboxylic anhydrides) as major Ni/C surface sites. The iron incorporation and the constitution of bimetallic NiFe/C catalyst achieved the development of basic sites. The intrinsic capacity of Fe species towards adsorbing CO_2 molecules might certainly play a role in the larger catalyst basicity's. Regarding the monometallic catalysts, superior surface basicity was exhibited by the bimetallic catalysts i.e., higher amounts of CO_2 and CO_{basic} species desorbed by NiFe/Al and NiFe/C, respectively.

3.5. Catalytic activity

The catalytic activity of the samples was evaluated for CO_2 methanation reaction at 60 L/gh and H_2:CO_2 ratio of 4 (Fig. 7). The CO_2 conversion values increased with the temperature for all the prepared samples. Both Ni/Al and Ni/C catalysts reached equilibrium conversions at 500 °C. Compared to Ni/C catalyst, Ni/Al exhibited better catalytic performances (ca. 8%) within the intermediate temperature range. For monometallic Ni catalysts, the role of the support is also clearly evidenced in terms of CH_4 and CO selectivity's. Ni/C catalyst showed significantly lower CH_4 selectivity's than Ni/Al. The higher CO selectivity variations observed for Ni/C catalyst as a function of the temperature might be related to its larger Ni particle sizes and low surface basicity.“. Only at the highest temperatures, Ni/C and Ni/Al samples showed analogous CH_4 selectivity. Along with the considerable lower dispersions exhibited by Ni/C catalysts, the absence of basic sites showed on the CO_2-TPD by Ni/C catalyst might explain such depleted CH_4 formations.

Please cite this article as: M. González-Castaño et al., Are Ni/ and Ni_5Fe_1/biochar catalysts suitable for synthetic natural gas production? A comparison with γ-Al_2O_3 supported catalysts, Green Energy & Environment, https://doi.org/10.1016/j.gee.2021.05.007

Table 3
H_2-TPR and CO_2-TPD quantification.

	H_2-TPR	CO_2-TPD			
	mol H_2/molNi	*CO_2 ($\mu mol/g_{cat}$)*	*CO_{acid} ($\mu mol/g_{cat}$)*	*$CO_{,basic}$ ($\mu mol/g_{cat}$)*	*Basic site density ($\mu mol/m^2$)*
Ni/Al	1.1	308.5	–	–	1.89
NiFe/Al	1.1	379.1	–	–	2.26
Ni/C	1.3	120.9	120.8	–	–
NiFe/C	1.2	140.8	139.8	144.2	0.20

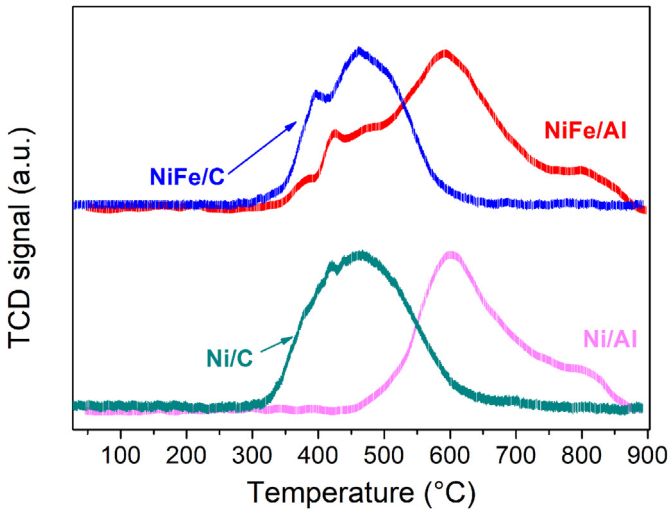

Fig. 5. H_2-TPR obtained for the synthesized catalysts.

The iron incorporation results on noticeable enhanced catalytic behaviors for both bimetallic supported catalysts. Indeed, NiFe/Al and NiFe/C described light−off curves shifted towards lower temperatures reaching the equilibrium conversions at 450 °C. Compared to their corresponding monometallic catalysts, ca. 25% higher CO_2 conversions were displayed by bimetallic samples within the intermediate temperature range. Although similar CH_4/CO selectivity's were described by Ni/Al and NiFe/Al supported catalysts, the Fe incorporation over the biochar support entails markedly improved CH_4 selectivity's. In fact, NiFe/C catalysts showed lower CO selectivity's than their homologous NiFe/Al sample.

Fig. 8A and B shows the effect of the H_2:CO_2 ratio on the CO_2 conversion and CH_4 selectivity for the catalyst series at 400 °C. Lower H_2:CO_2 ratios resulted in decreased CO_2 conversions for all catalysts which displayed no significant conversions H_2:$CO_2 = 1$. Besides, similar trends were exposed as a function of the active phase i.e. Ni or Ni−Fe. Compared to monometallic Ni catalysts, the larger conversions drops displayed by NiFe bimetallic catalysts when the H_2:CO_2 ratio decreased from 4 to 3 suggest that the catalytic improvement attained by Ni_5Fe_1 alloy is strongly affected by the H_2 partial pressures, i.e. H_2 surface coverages. Besides, higher H_2 partial pressures resulted in slightly higher CH_4 selectivity's being this increment more accentuated for Ni/C catalyst. Furthermore, the evolution of the CO_2 conversion and CH_4 selectivity observed as a function of the space velocity is showed in Fig. 8C and D, respectively. Lower contact times result in decreased CO_2 conversions for all the samples. Once again, slightly higher CO_2 conversion drops were observed for the NiFe catalysts compared to the Ni-samples. Compared to alumina catalysts, biochar-based systems showed slightly higher CH_4 selectivity drops. The detrimental effect of the space velocity concerning the CH_4 selectivity was also particularly important for Ni/C catalyst. The stronger influence of the H_2/CO_2 ratio and space velocity observed for the biochar supported catalysts might be related to the larger particles sizes.

Table 4 depicts the activation energies, specific reaction rates and TOFs estimated for the catalyst series. The comparable reaction rates exhibited by biochar- and alumina-based catalysts establish biochar as a competitive renewable support. As expected, superior reaction rates were attained by the NiFe supported catalysts compared to the monometallic Ni ones. In terms of TOFs values, NiFe/C catalyst displayed the highest specific activity. Thus, NiFe/C catalyst exhibited analogous CO_2 conversion than NiFe/Al ones' despite of the

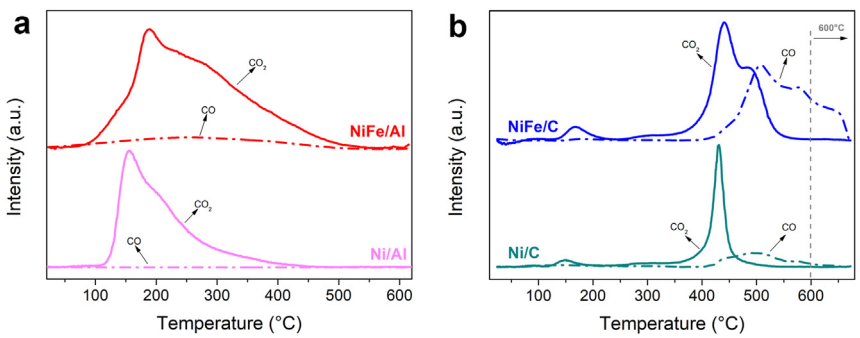

Fig. 6. CO_2-TPD obtained for the reduced catalysts followed by a mass spectrometer: a) Ni/Al and NiFe/Al and b) Ni/C and NiFe/C catalysts.

Please cite this article as: M. González-Castaño et al., Are Ni/ and Ni_5Fe_1/biochar catalysts suitable for synthetic natural gas production? A comparison with γ-Al_2O_3 supported catalysts, Green Energy & Environment, https://doi.org/10.1016/j.gee.2021.05.007

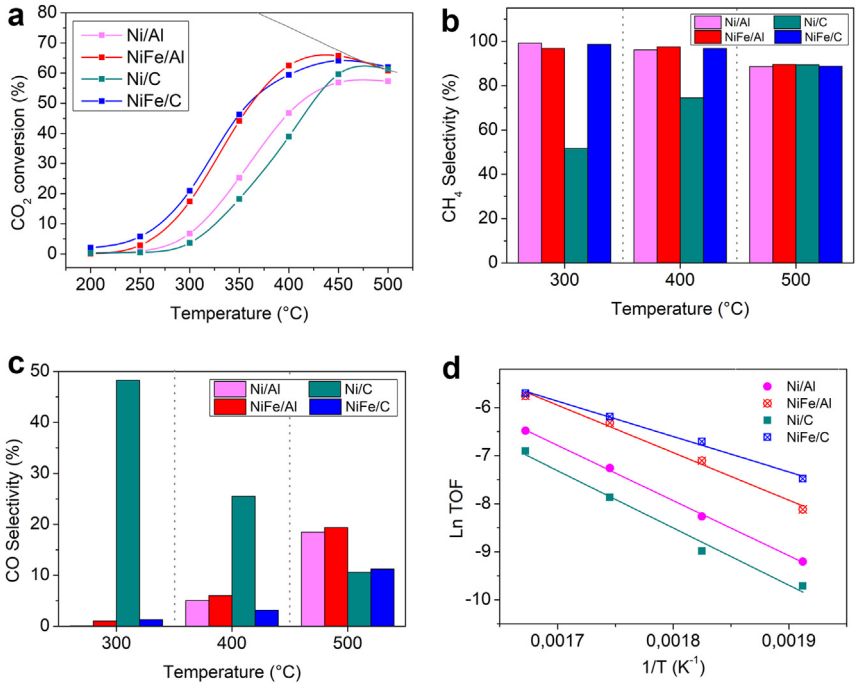

Fig. 7. Catalytic activity obtained at 60 L/gh and H_2:CO_2 = 4: a) CO_2 conversion; b) CH_4 selectivity c) CO selectivity and d) Arrhenius's plot for CO_2 conversion and CO formation (inset).

considerably lower number of exposed active sites. Considering the comparable structural features observed for Ni_5Fe_1 alloy in both from XRD data, variations on the TOFs must be related to NiFe–C support interactions. For the Ni/Al catalyst, the activation energies for the CO_2 conversion ($Ea_{CO2,c}$) were 95.4 kJ/mol being those in agreement with previously reported values [45,46]. Compared to Ni/C catalyst, the slightly higher activation energies for the CO_2 conversion estimated for the Ni/Al catalyst agrees with the better displayed performances. The enhanced catalyst performances described by NiFe supported catalysts were also evidenced on the calculated $Ea_{CO2,c}$ being noticeably lower for the NiFe/C catalyst.

3.6. XPS analysis for aged NiFe/Al and NiFe/C catalysts

XPS analysis of aged samples was employed to evaluate the impact of the support on the surface properties displayed by the NiFe alloys. With that aim, samples were reduced under H_2 atmosphere at 600 °C and subjected to diluted feed streams with H_2:CO_2 = 4 ratios. Significant lower signal to noise ratios were measured for the NiFe/C sample. Fig. 9A and C compares the normalized Ni2p and Fe2p spectra displayed by the calcined and aged NiFe/C and NiFe/Al samples. While comparable Fe2p spectra were observed for the fresh and aged samples, the constitution of partially reduced Ni phases on both catalysts surfaces results in significant changes in the Ni 2p spectra showed by as-prepared and spent samples. Thus, a new contribution appears at ~852.5 eV, indicating the presence of metallic Ni^0 [47]. For the spent NiFe/Al catalyst, probably due to the optimal noise to signal ratios, the presence of metallic Fe could be observed. Inhere, Ni/Fe ratios of 5 were estimated being this in very good agreement to the XRD data. Furthermore, both Ni and NiO phases were observed for both NiFe/Al and NiFe/C samples. Despite characteristic uncertainties of XPS ex-situ analysis, mixed Ni/NiO mixed populations are usually reported for post-reacted samples under mildly oxidizing reaction conditions [48]. Aged NiFe/C and NiFe/Al samples showed Ni:NiO ratio estimations of 40 and 34%, respectively. On the contrary, NiFe/C sample showed higher Fe^{3+}/Fe^{2+} ratios (1.55) than the corresponding NiFe/Al (1.33).

3.7. Catalytic stability of bimetallic NiFe catalysts

Finally, the catalytic activity displayed by the NiFe/C and NiFe/Al catalysts at 400 °C during about 60 h (Fig. 10). Stable performances with no observable changes regarding CO_2 conversion nor selectivity to CH_4 were attained by both systems. The present outcome agrees with the finding reported elsewhere [49], where the use of bimetallic catalysts over carbon supported catalysts was found beneficial for the catalyst stability. For NiFe catalysts, the enhanced resistances against carbon deposits [18], the hindered oxidation of Ni^0 observed in XPS spectroscopy, and the inhibited Ni agglomeration issues suggested from the lower particle size distribution account for the observed stable performances.

4. Discussion

Employing alumina based catalysts as reference systems, Ni and NiFe biochar catalysts have been characterized and tested for producing SNG via CO_2 methanation reaction.

Please cite this article as: M. González-Castaño et al., Are Ni/ and Ni_5Fe_1/biochar catalysts suitable for synthetic natural gas production? A comparison with γ-Al_2O_3 supported catalysts, Green Energy & Environment, https://doi.org/10.1016/j.gee.2021.05.007

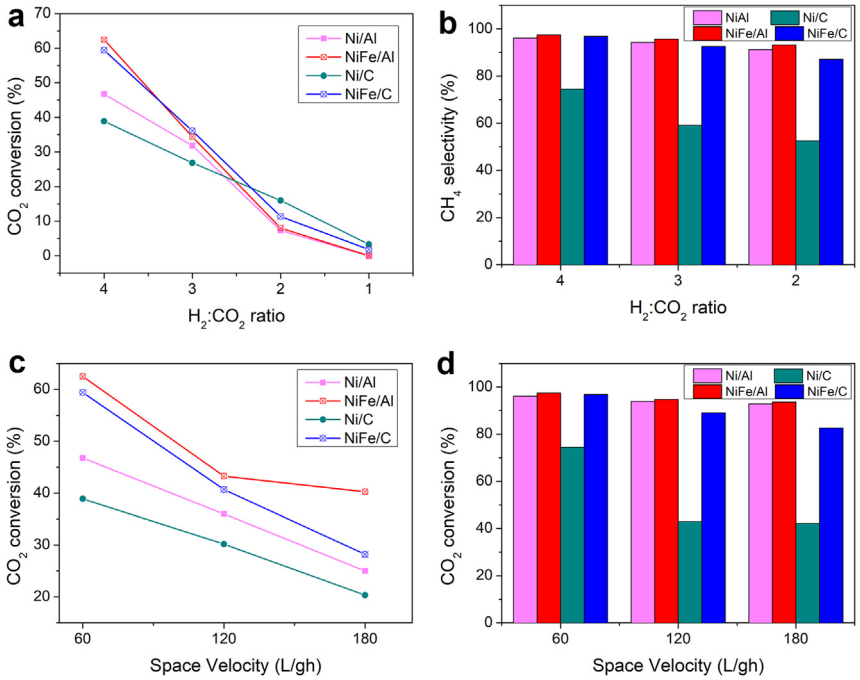

Fig. 8. Effect of H_2:CO_2 ratio at 400 °C and 60 L/gh: A) CO_2 conversion; B) CH_4 selectivity; Effect of the space velocity at 400 °C and H_2:CO_2 ratio = 4: C) CO_2 conversion; D) CH_4 selectivity.

Several differences concerning particle sizes, redox properties, and surface basicity were found as a function of the employed support. Still, in terms of absolute CO_2 conversions and catalyst stabilities, the rather smaller differences observed between both dispersing matrixes points out the importance of the active phase and establishes porous biochar materials as suitable supports.

Concerning bare Ni catalysts, higher Ni particle sizes were developed over biochar support compared to alumina catalysts. Such higher particle sizes should be attributed to weaker Ni support interactions over biochar surfaces, which results in significant differences concerning the metal reducibility's behavior e.g. H_2-TPR profiles evidenced NiO reductions centered at 600 °C for the Ni/Al catalyst and at 400 °C for the Ni/C catalyst. Another important variation concerns the surface basicity exhibited by Ni/Al and Ni/C catalysts. In this sense, the amount of CO_2 species desorbed on the CO_2-TPD for the Ni/Al pointed out the presence of surface weak and medium strength basic sites with concentrations (1.89 μmol/m^2) similar to those reported in the literature [5]. On the contrary, no species associated with basic sites were desorbed from the Ni/C surface during the CO_2-TPD experiment. Compared to Ni/Al catalyst, the lower TOFs and significantly depleted CH_4 selectivity's exhibited by Ni/C catalyst must be mainly related to the lack of basic sites on the Ni/C surface. For CO_2 methanation, the hydrogenation of CO_2* or CO* activated molecules is considered the rate-limiting step [50]. In this sense, favored electrons delocalization around adsorbed CO molecules, for instance by adding H from the support, entail promoted catalytic performances [51]. Therefore, the overall catalyst reaction rate relies on the hydrogen species available on the surrounding of the active sites, which at the same time come determined by H_2 coverage and transport properties [52]. Employing DFT calculations, Psofogianakis et al. [53] demonstrated that the transport of H species over graphitic carbon surfaces increases with the number of oxygen surface sites. Thus, the depleted H_2 surface dynamics presented by Ni/C sample account not only for the lower TOFs depicted by Ni/C but also for the poor CH_4 selectivity. Furthermore, a certain particle size effect could be argued. For Ni silica catalysts, Vogt et al. [50] claimed that CO_{ads} intermediates species exhibited much stronger adsorptions over larger Ni particles. Although the structure-sensitivity proposed for particle sizes ranging from 1 to 6 nm might be to somehow limited for larger particles, the superior CO selectivity might be also related to the stronger CO–Ni interactions established over larger Ni sizes.

Moreover, the constitution of NiFe bimetallic catalysts reported enhanced catalyst performances for both supports. From XRD data, constricted crystallite growths and Ni^0 diffraction lines shifted towards lower 2θ angles suggested the

Table 4
Specific reaction rates, TOFs, and activation energies attained for the different catalysts.

	Rate (mmolCO_2/s g_{Ni})		TOF (10^3 s^{-1})	Activation energy
	300 °C	400 °C	300 °C	$Ea_{CO2,c}$ *(KJ/mol).*
Ni/Al	5.38	36.95	0.81	95.4
NiFe/Al	13.77	49.44	1.52	82.1
Ni/C	2.92	31.01	0.63	99.0
NiFe/C	15.70	44.57	3.12	61.1

Please cite this article as: M. González-Castaño et al., Are Ni/ and Ni_5Fe_1/biochar catalysts suitable for synthetic natural gas production? A comparison with γ-Al_2O_3 supported catalysts, Green Energy & Environment, https://doi.org/10.1016/j.gee.2021.05.007

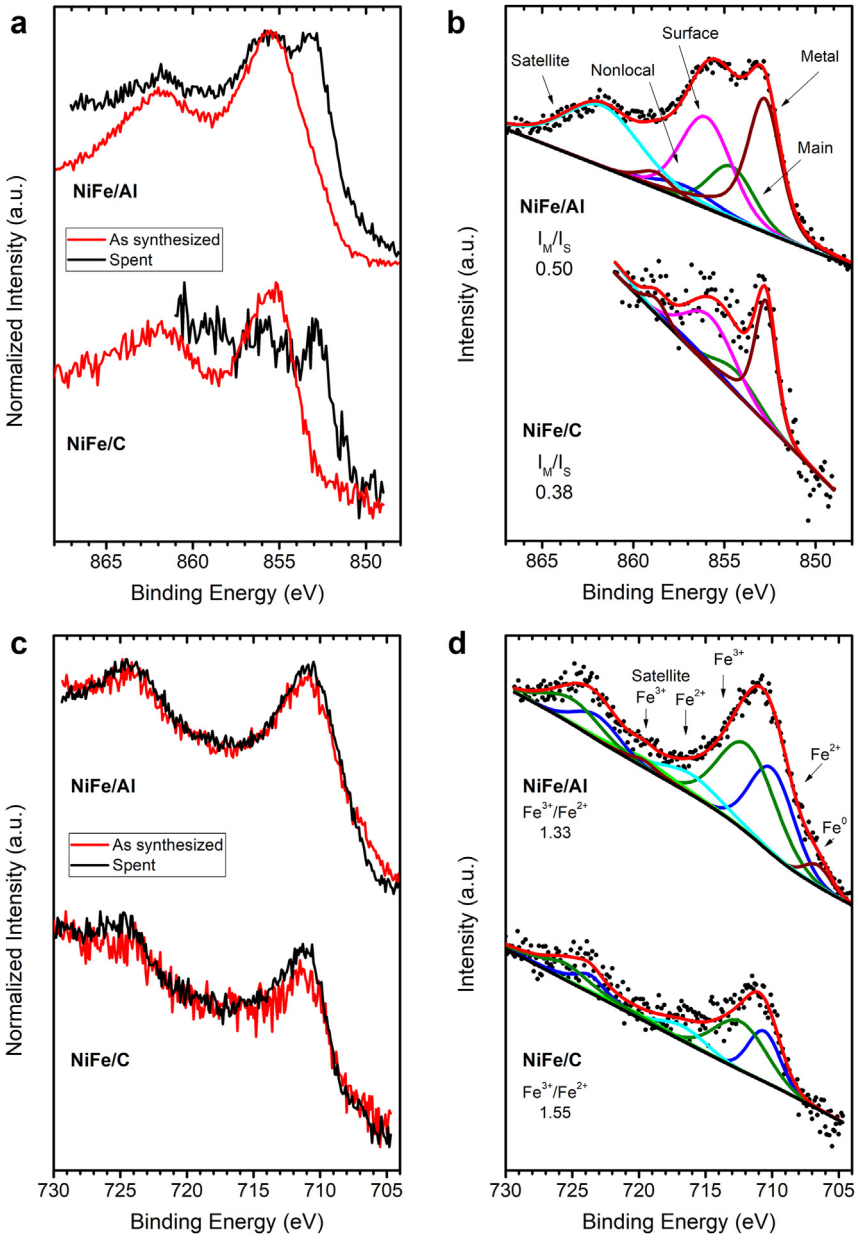

Fig. 9. XPS spectra obtained for the as-prepared and aged Ni_5Fe_1/C and Ni_5Fe_1/Al catalysts during 2 h at 400 °C under diluted H_2:CO_2 = 4: a) as-prepared and spent Ni2p spectra; b) Ni2p fitting of the spent samples; c) as-prepared and spent Fe2p spectra and d) Fe 2p fitting of the spent samples.

constitution of NiFe alloys. Based on Vegard's law, analogous Ni_5Fe_1 alloys were constituted for both NiFe/Al and NiFe/C catalysts. The decreased particle sizes observed for Ni_5Fe_1 catalysts underlined FeO_x species acting as a textural promoter. Similar to bare Ni catalysts, larger particle sizes and wider distributions were found for NiFe/C (10 nm) compared to NiFe/Al (6 nm). Respect monometallic Ni systems, NiFe catalysts also reported superior amounts of species desorbed during CO_2-TPD, i.e. increased surface basicity. It is worth remarking that the iron incorporation did provoke the constitution of a significant number of new basic sites on the surface of the NiFe/C catalyst. Compared to Ni/C catalyst for which no basic sites were detected, the superior CH_4 selectivity's achieved by NiFe/C could be related to the constitution of basic sites. Being capable of efficiently transport the H species [53], basic surface active sites should favour not only the CO_2 activation but also, the subsequent hydrogenation of the constituted reaction intermediates. With NiFe/Al and NiFe/C exhibiting analogous activities in terms of CO_2 conversions, ca. 2 times larger specific activities per Ni site exposed (TOFs) were showed by NiFe/C catalyst. Under mildly oxidizing atmospheres due to the presence of CO_2, Du et al. [48] observed the partial oxidation of Ni species. Being the Ni^0 the main active site for CO_2 methanation conditions, deteriorated catalysts performance are intimately associated with the lower Ni/NiO surface ratios established under reaction conditions. For NiFe alloys, the role of iron species has been related to increased Ni^0 populations on the catalyst surface and optimal

Please cite this article as: M. González-Castaño et al., Are Ni/ and Ni_5Fe_1/biochar catalysts suitable for synthetic natural gas production? A comparison with γ-Al_2O_3 supported catalysts, Green Energy & Environment, https://doi.org/10.1016/j.gee.2021.05.007

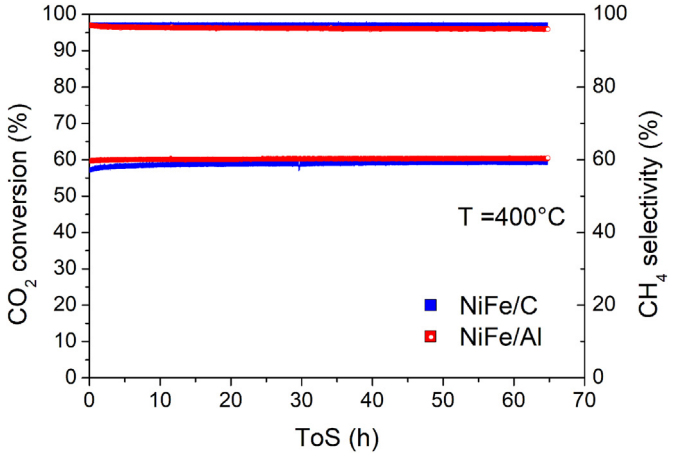

Fig. 10. Catalytic stability exhibited by NiFe/C and NiFe/Al catalysts at 400 °C, 60 L/gh and H_2:CO_2 = 4.

CO activation energies due to weaker metal support interactions. Mebrahtu et al. [54] associated the catalytic improvements of Fe species to hindered the constitution of $Ni(OH)_2$ species resulting in higher Ni^0 populations. In that manner, Fe species act as a protecting sacrificial agent which ensued higher Ni metal fractions [55]. Thus, the improved TOFs depicted by NiFe/C catalyst should be associated with higher Ni/NiO fractions estimated by XPS analysis over the spent samples. The weaker metal NiFe–C support interactions established might support the stabilization of higher Ni^0 populations attaining improved catalyst performances. The higher Fe^{3+}/Fe^{2+} populations discerned for NiFe/C catalysts in XPS analysis reinforces the protective role of Fe in NiFe alloys.

5. Conclusions

This work establishes a meaningful comparison between Al_2O_3 and biochar as supports for Ni and NiFe catalysts applied to CO_2 methanation reaction. While monometallic Ni/Al catalyst depicted superior catalyst performances than Ni/C system, the constitution of analogous Ni_5Fe_1 alloys lead to superior TOFs over biochar supports. The potentiality of biochar-based catalysts for CO_2 methanation processes, as an alternative to Al_2O_3 catalysts, strongly relies on the basic properties achieved on the biochar surface. The development of basic sites on the biochar surface was found dependent on the nature of the active phase i.e. the presence of basic sites on the biochar surface was only achieved for the NiFe/C catalyst. In this sense, the lower TOFs and depleted CH_4 selectivity's exhibited by Ni/C were mostly associated with the absence of basic sites on the catalyst surface. For bimetallic NiFe catalysts, the superior TOF observed for NiFe/C catalyst was associated with: i) improved surface basicity, which might promote the CO_2 activations and H transport properties; and ii) the higher Ni^0/NiO ratios contents, allowed by efficient NiFe alloys weakly interacting with the carbon support.

Declaration of competing interest

The authors declare that they have no known competing financial interests or personal relationships that could have appeared to influence the work reported in this paper.

Acknowledgments

Acknowledgments to Sasol for providing the gamma-Al_2O_3 support.

Appendix A. Supplementary data

Supplementary data to this article can be found online at https://doi.org/10.1016/j.gee.2021.05.007.

References

[1] J.C. Navarro, M.A. Centeno, O.H. Laguna, J.A. Odriozola, Catalysts 8 (2018) 1–25.
[2] (n.d.).
[3] M.A.A. Aziz, A.A. Jalil, S. Triwahyono, M.W.A. Saad, Chem. Eng. J. 260 (2015) 757–764.
[4] D. Pandey, G. Deo, J. Ind. Eng. Chem. 33 (2016) 99–107.
[5] C. Italiano, J. Llorca, L. Pino, M. Ferraro, V. Antonucci, A. Vita, Appl. Catal. B Environ. 264 (2020) 118494.
[6] P. Frontera, A. Macario, M. Ferraro, P.L. Antonucci, Catalysts 7 (2017) 1–28.
[7] X. Lin, S. Wang, W. Tu, Z. Hu, Z. Ding, Y. Hou, R. Xu, W. Dai, Catal. Sci. Technol. 9 (2019) 731–738.
[8] S. Utgenannt, F. Hansen, O. Klepel, S. Jarczewski, A. Wach, P. Kütrowski, Catal. Today 249 (2015) 38–44.
[9] P. Zhang, L. Wang, S. Yang, J.A. Schott, X. Liu, S.M. Mahurin, C. Huang, Y. Zhang, P.F. Fulvio, M.F. Chisholm, S. Dai, Nat. Commun. 8 (2017).
[10] L.R. Winter, E. Gomez, B. Yan, S. Yao, J.G. Chen, Appl. Catal. B Environ. 224 (2018) 442–450.
[11] J. Wu, Z. Jin, B. Wang, Y. Han, Y. Xu, Z. Liang, Z. Wang, Ind. Eng. Chem. Res. (2019).
[12] A. Alarcón, J. Guilera, J.A. Díaz, T. Andreu, Fuel Process. Technol. 193 (2019) 114–122.
[13] S.A. Kondrat, P.J. Smith, P. Peter, P.A. Chater, J.H. Carter, D.J. Morgan, E.M. Fiordaliso, J.B. Wagner, T.E. Davies, L. Lu, J.K. Bartley, S.H. Taylor, M.J. Rosseinsky, G.J. Hutchings, M.S. Spencer, C.J. Kiely, G.J. Kelly, W. Colin, (2016).
[14] W.L. Vrijburg, G. Garbarino, W. Chen, A. Parastaev, A. Longo, E.A. Pidko, E.J.M. Hensen, J. Catal. 382 (2020) 358–371.
[15] D. Pandey, G. Deo, J. Mol. Catal. Chem. 382 (2014) 23–30.
[16] J. Sehested, K.E. Larsen, A.L. Kustov, A.M. Frey, T. Johannessen, T. Bligaard, M.P. Andersson, J.K. Nørskov, C.H. Christensen, Top. Catal. 45 (2007) 9–13.
[17] B. Mutz, P. Sprenger, W. Wang, D. Wang, W. Kleist, J.D. Grunwaldt, Appl. Catal. Gen. 556 (2018) 160–171.
[18] S.M. Kim, P.M. Abdala, T. Margossian, D. Hosseini, L. Foppa, A. Armutlulu, W. Van Beek, A. Comas-Vives, C. Copéret, C. Müller, J. Am. Chem. Soc. 139 (2017) 1937–1949.
[19] K. Ray, G. Deo, Appl. Catal. B Environ. 218 (2017) 525–537.
[20] A.I. Tsiotsias, N.D. Charisiou, I.V. Yentekakis, M.A. Goula, Nanomaterials 11 (2021) 1–34.
[21] L. Pastor-Pérez, E. Le Saché, C. Jones, S. Gu, H. Arellano-Garcia, T.R. Reina, Catal. Today 317 (2018) 108–113.

[22] J. Ren, X. Qin, J.Z. Yang, Z.F. Qin, H.L. Guo, J.Y. Lin, Z. Li, Fuel Process. Technol. 137 (2015) 204–211.
[23] A.C. Lausche, A. Medford, J.K. Norskov, F. Studt, Eng. Sci. Fundam. 2 (2013) 893–894, 2013 - Core Program. Area 2013 AIChE Annu. Meet. Glob. Challenges Eng. a Sustain. Futur.
[24] S. Hwang, U.G. Hong, J. Lee, J.H. Baik, D.J. Koh, H. Lim, I.K. Song, Catal. Lett. 142 (2012) 860–868.
[25] C. Liang, Z. Ye, D. Dong, S. Zhang, Q. Liu, G. Chen, C. Li, Y. Wang, X. Hu, Fuel 254 (2019) 115654.
[26] M.A. Serrer, K.F. Kalz, E. Saraçi, H. Lichtenberg, J.D. Grunwaldt, ChemCatChem 11 (2019) 5018–5021.
[27] B. Mutz, M. Belimov, W. Wang, P. Sprenger, M.A. Serrer, D. Wang, P. Pfeifer, W. Kleist, J.D. Grunwaldt, ACS Catal. 7 (2017) 6802–6814.
[28] T.K. Campbell, J.L. Falconer, Appl. Catal. 50 (1989) 189–197.
[29] L.M. Gandia, M. Montes, Jounal Catal 145 (1993) 276–288.
[30] G. Bergeret, P. Gallezot, Handb. Heterog. Catal. (2008) 738–765.
[31] R.J.O. Mossanek, I. Preda, M. Abbate, J. Rubio-Zuazo, G.R. Castro, A. Vollmer, A. Gutiérrez, L. Soriano, Chem. Phys. Lett. 501 (2011) 437–441.
[32] T.C. Lin, G. Seshadri, J.A. Kelber, Appl. Surf. Sci. 119 (1997) 83–92.
[33] I. Preda, R.J.O. Mossanek, M. Abbate, L. Alvarez, J. Méndez, A. Gutiérrez, L. Soriano, Surf. Sci. 606 (2012) 1426–1430.
[34] D. Torres, J.L. Pinilla, I. Suelves, Catalysts 8 (2018).
[35] C.P. Kempter, Phys. Status Solidi 18 (1966) K117–K118.
[36] M. González-Castaño, S. Ivanova, T. Ioannides, M.A. Centeno, J.A. Odriozola, Catal. Sci. Technol. 7 (2017) 1556–1564.
[37] J.L. Santos, P. Mäki-Arvela, A. Monzón, D.Y. Murzin, M.Á. Centeno, Appl. Catal. B Environ. 268 (2020) 118423.
[38] J.L. Santos, P. Mäki-Arvela, J. Wärnå, A. Monzón, M.A. Centeno, D.Y. Murzin, Appl. Catal. B Environ. 268 (2020) 118425.
[39] J.L. Santos, M.A. Centeno, J.A. Odriozola, J. Anal. Appl. Pyrolysis 148 (2020) 104821.
[40] P. Kim, J.B. Joo, H. Kim, W. Kim, Y. Kim, I.K. Song, J. Yi, Catal. Lett. 104 (2005) 181–189.
[41] P. Michorczyk, P. Kuśtrowski, L. Chmielarz, J. Ogonowski, React. Kinet. Catal. Lett. 82 (2004) 121–130.
[42] D. Tian, Z. Liu, D. Li, H. Shi, W. Pan, Y. Cheng, Fuel 104 (2013) 224–229.
[43] M.A. Fraga, E. Jordão, M.J. Mendes, M.M.A. Freitas, J.L. Faria, J.L. Figueiredo, J. Catal. 209 (2002) 355–364.
[44] F. Coloma, A. Sepúlveda-Escribano, J.L.G. Fierro, F. Rodríguez-Reinoso, Langmuir 10 (1994) 750–755.
[45] T. Van Herwijnen, H. Van Doesburg, W.A. De Jong, J. Catal. 28 (1973) 391–402.
[46] F. Koschany, D. Schlereth, O. Hinrichsen, Appl. Catal. B Environ. 181 (2016) 504–516.
[47] H.W. Nesbitt, D. Legrand, (2000) 357–366.
[48] G. Du, S. Lim, Y. Yang, C. Wang, L. Pfefferle, G.L. Haller, J. Catal. 249 (2007) 370–379.
[49] G. Monnier, S. Ivanova, J.L. Santos, C. Le, M.A. Centeno, A. Odriozola (2020) 5.
[50] C. Vogt, E. Groeneveld, G. Kamsma, M. Nachtegaal, L. Lu, C.J. Kiely, P.H. Berben, F. Meirer, B.M. Weckhuysen, Nat. Catal. 1 (2018) 127–134.
[51] C. Vogt, M. Monai, E.B. Sterk, J. Palle, A.E.M. Melcherts, B. Zijlstra, E. Groeneveld, P.H. Berben, J.M. Boereboom, E.J.M. Hensen, F. Meirer, I.A.W. Filot, B.M. Weckhuysen, Nat. Commun. 10 (2019) 1–10.
[52] M. González-Castaño, E. Le Saché, S. Ivanova, F. Romero-Sarria, M.A. Centeno, J.A. Odriozola, Appl. Catal. B Environ. 222 (2018) 124–132.
[53] G.M. Psofogiannakis, G.E. Froudakis, J. Am. Chem. Soc. 131 (2009) 15133–15135.
[54] C. Mebrahtu, F. Krebs, S. Perathoner, S. Abate, G. Centi, R. Palkovits, Catal. Sci. Technol. 8 (2018) 1016–1027.
[55] G. Giorgianni, C. Mebrahtu, M.E. Schuster, A.I. Large, G. Held, P. Ferrer, F. Venturini, D. Grinter, R. Palkovits, S. Perathoner, G. Centi, S. Abate, R. Arrigo, Phys. Chem. Chem. Phys. 22 (2020) 18788–18797.

Please cite this article as: M. González-Castaño et al., Are Ni/ and Ni_5Fe_1/biochar catalysts suitable for synthetic natural gas production? A comparison with γ-Al_2O_3 supported catalysts, Green Energy & Environment, https://doi.org/10.1016/j.gee.2021.05.007